Department of Energy
Office of Energy Efficiency and Renewable Energy
Solid State Lighting Core Technologies

Final Report
(September, 2013)
Title:
High Efficiency Organic Light Emitting Devices for Lighting
Work Performed Under Agreement:
DE-EE0001522

Submitted By:
University of Florida
Department of Materials Science and Engineering
P. O. Box 116400
Gainesville, FL 32611-6400

Principal Investigator:
Franky So
University of Florida
Phone: (352) 846-3790
Fax: (352) 846-1182
E-mail: fso@mse.ufl.edu

Co-Principal Investigators
Nelson Tansu
James F. Gilchrist
Lehigh University
E-mail: Tansu@Lehigh.Edu

Submitted To:
U. S. Department of Energy
National Energy Technology Laboratory
Project Officer: Joel Chaddock
E-mail: Joel.Chaddock@netl.doe.gov

DISCLAIMER

This report was prepared as an account of work sponsored by an agency of the United States Government. Neither the United States Government nor any agency thereof, nor any of their employees, makes any warranty, express or implied, or assumes any legal liability or responsibility for the accuracy, completeness, or usefulness of any information, apparatus, product, or process disclosed, or represents that its use would not infringe privately owned rights. Reference herein to any specific commercial product, process, or service by trade name, trademark, manufacturer, or otherwise does not necessarily constitute or imply its endorsement, recommendation, or favoring by the United States Government or any agency thereof. The views and opinions of authors expressed herein do not necessarily state or reflect those of the United States Government or any agency thereof.

A. Project Objective:

Incorporate internal scattering layers and microlens arrays in high efficiency OLED to achieve up to 70% EQE.

B. Technical Approach and Work Plan

1. Development of high efficiency white OLEDs
    i. Fabrication and characterization of white OLEDs
    ii. Characterization and optimization of charge generation layers
    iii. Fabrication and optimization of tandem OLEDs
2. Fabrication and optimization of convex microlens arrays
    i. Simulation of OLEDs with convex microlens arrays
    ii. Fabrication and optimization of convex microlens arrays
3. Fabrication and optimization of concave microlens arrays
    i. Simulation of OLEDs with concave microlens arrays
    ii. Fabrication and optimization of concave microlens arrays
4. Fabrication of OLEDs incorporating convex and concave microlens arrays
    i. Fabrication of OLEDs with convex microlens arrays
    ii. Fabrication of OLEDs with concave microlens arrays
    iii. Fabrication and optimization of OLEDs with both concave and convex microlens arrays

III.1 Summary

We fabricated OLEDs on microlens array substrates. We developed an imprinting process to fabricate OLEDs on 0.5 μm and 1.0 μm microlens array substrates. With a perfect self-assembled micro sphere array to form the grating structure for light extraction, it is expected that the light emission profile is wavelength dependent with a strong angle dependence. Because of the defects present in the microlens array, the light emission profile from the resulting OLEDs is almost lambertian due to the so-called “defective grating”. As a result, we were able to obtain an enhancement of 2X in power efficiency. Using a macro lens to further extract the substrate mode, we were able to obtain a 3X enhancement in light extraction.

The optimized OLEDs with phosphorescent dopant of $Ir(ppy)_3$ showed 49 cd/A and 33 lm/W in current and power efficiencies. With the 0.5-μm-diamter silica array, the current and power efficiencies were improved to 78 cd/A and 72 lm/W, giving rise to 60% and 120% enhancements, respectively. With a hemisphere lens, the total power efficiency of the grating device was enhanced by a factor of ~3.7.

With the 0.4-μm-diamter silica array, the grating devices showed the lower enhancement of 46% in the current efficiency over the reference than the 0.5 μm grating device due to the lower depth of the corrugated structure.

III.2 Fabrication of Microlens Arrays with Various Diameters

In order to optimize the light extraction efficiency in OLED devices, we have developed the process to optimize the microsphere / microlens deposition with diameters ranging from 100 nm, 500 nm, and 1 μm. The development of microlens arrays with small diameters are of great importance, in particular to achieve a larger escape cone for extraction of photons from the OLED devices. The use of rapid convective deposition process for binary particle depositions was employed in the fabrication of microlens arrays with small diameters. The SEM images of the microlens arrays with varying diameters were shown in Figure 1.

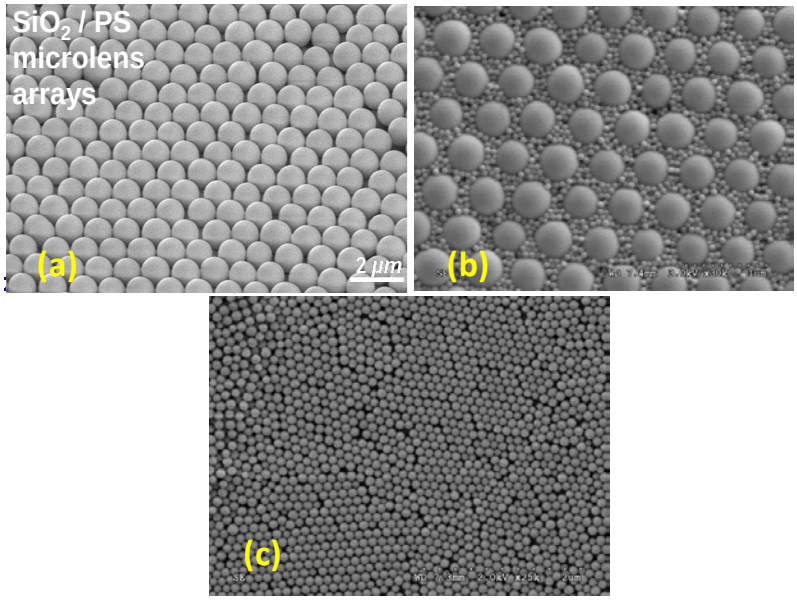

Figure 1: Scanning electron microscopy images for monolayer SiO2 / PS microlens arrays deposited by rapid convective deposition method with diameters of (a) 1 μm, (b) 500 nm, and (c) 100 nm.

To optimize the light extraction efficiency and far field radiation pattern in OLED devices, we fabricated SiO_2/PS microlens arrays with various aspect ratios. The use of rapid convective deposition and high temperature treatment enable the tuning of the thickness of the PS structure, which in turn resulted in microlens arrays with various aspect ratio (Figure 2).

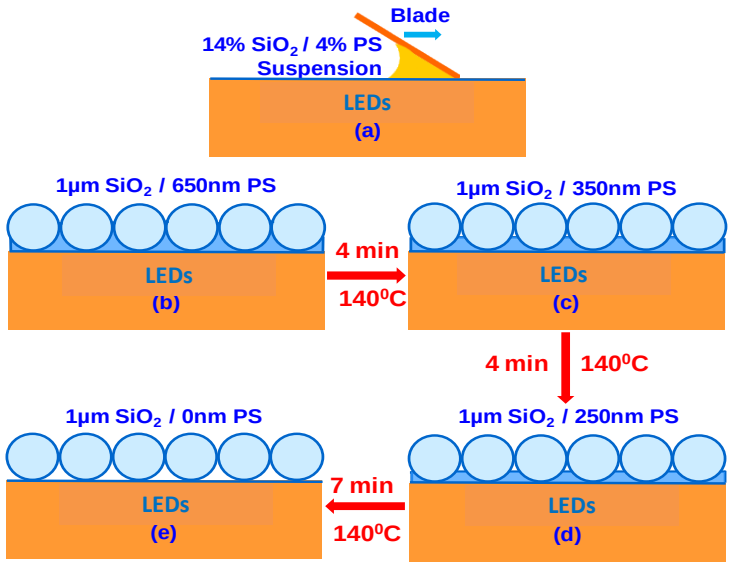

Figure 2: (a) Cross-sectional schematics of the rapid convective deposition of SiO_2 / PS microlens arrays, and (b)-(e) fabrication process flows of SiO_2 / PS microlens with various PS thicknesses via high temperature annealing at 140 ^{0}C.

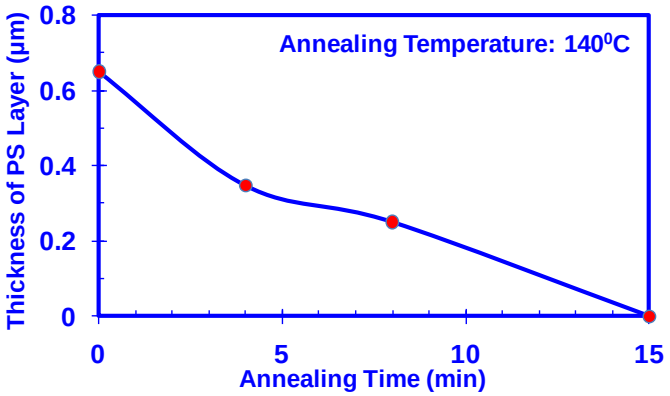

Figure 3: PS thickness vs annealing time of SiO_2 / PS microlens arrays deposited by the RCD of 14% SiO_2 / 4% PS binary suspension.

From our studies, we found that the melting of the PS layer via high temperature treatment follows a relatively quasi linear relation with annealing time. As shown in Figure 3, the PS thickness in the SiO_2/PS microlens arrays is in quasi-linear proportion to the annealing time at the annealing temperature of 140 ^{0}C. Hence arbitrary PS thicknesses between 0 nm to 650 nm can be obtained, depending on the dimension of interest.

To investigate the surface topographies and planar PS thickness of the SiO_2/PS microlens arrays, scanning electron microscopy (SEM) [Hitachi 4300] was used to examine the samples after RCD and annealing [Figures 2(a)-2(e)]. Figures 4(a)- 4(d) show the cross-sectional and 45°-tilted SEM images of the SiO_2/PS microlens arrays on top of the LED with PS thicknesses of 0 nm, 250 nm, 350 nm, and 650 nm, respectively. From Figures 4(a)-4(d), the SEM images clearly show the fabrication of the convex microlens arrays with various aspect ratios. As shown in Figure 4(b), by annealing the

sample at 140 ^{0}C for 4 minutes, the evaporation process of PS led to a reduction of PS thickness to 350 nm. The PS layer thickness can be further reduced to 250 nm with 4 additional minutes of annealing [Figure 4(c)]. Finally, the PS layer was completely evaporated off with total annealing time of 15 minutes [Figure 4(d)].

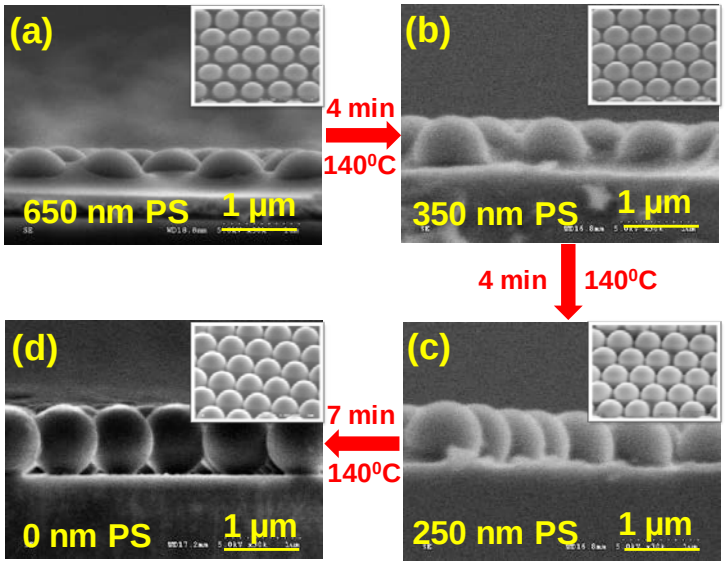

Figure 4: SEM images for the 1.0-µm SiO_2 / PS microlens arrays with PS thicknesses of (a) 650 nm, (b) 350 nm, (c) 250 nm, (d) 0 nm, with the insets showing the images tilted at 45^0.

In addition, we have also implemented this approach to fabricate GaN-based LEDs using microlens arrays with various aspect ratios. From our finding, it is evident that the implementation of the optimized PS layer thickness in the SiO_2/PS microlens arrays led to an enhancement in the output power and light extraction efficiency, in particular in enhancing the diffused light extraction at a large angular direction. This comparison supports the observation in the EL measurements that the controllability of PS layer thickness is critical in extracting and diffusing the light towards a larger angular direction.

Optimization and FDTD Analysis for Smaller Diameter Microlens OLED Devices

From this finding, the use of smaller diameter microlens arrays show a good potential in achieving optimized light extraction efficiency in OLEDs. In the subsequent work, we continue to optimize the deposition of microlens arrays with diameter specifically in the 250-nm up to 500 nm (250 nm, 300 nm, 400 nm) for implementation in OLED devices. The use of microlens arrays with 400-nm appear to be of great interest based on preliminary simulation data. In addition, our group will also work on the computational electromagnetics by using FDTD analysis to achieve optimized dimensions for experimental implementation in the OLED device structures.

III.3 Incorporation process of silica sphere array to OLED device

To fabricate OLED devices on microlens array substrates, imprinting process was used. The silica sphere array template was prepared on glass substrates by rapid convective deposition process of suspensions consisting of 1.0- and 0.5-μm-diameter silica and 100-nm-diameter polystyrene spheres. After heat treatment, the polystyrene spheres were melted to form a thin film embedded with a monolayer of silica spheres, thereby forming corrugated structures with periodicities corresponding to the size of the silica spheres. However, this deposition process inevitably accompanies defects such as voids in the structure despite of local hexagonal-closed-packed (HCP) structure, as shown in Fig. 5. Since the defect sites can lead to electrical-short paths when the OLED devices are fabricated directly on the silica sphere array template, it is important to reduce the surface roughness around the defects of the array pattern to prevent electrical shorting problems in the corrugated OLED devices.

To solve this problem, we produced a PDMS replica by pouring PDMS material on the silica array template cured at 60°C for 2 hours, as shown in Fig. 6. While most of the array pattern is transferred to the PDMs replica, the PDMS material is unable to completely fill the valley parts between spheres as well as the defect sites because of its viscosity, smoothening the surface of the template and therefore reducing the depth of the array. By imprinting process with the PDMS replica, the UV-curable resin layer with the silica array pattern was fabricated on glass by imprinting process. Finally, while the depths of the silica array templates were 180~190 and 70~80 nm for the 1.0 and 0.5 μm templates, respectively, the depths of the corrugated resin layers imprinted from the template were reduced slightly to 170~180 and 60~70 nm respectively, but the devices on the corrugated resin layers showed stable and repeatable electrical performance without electrical-short problems because of the smoothened defect sites.

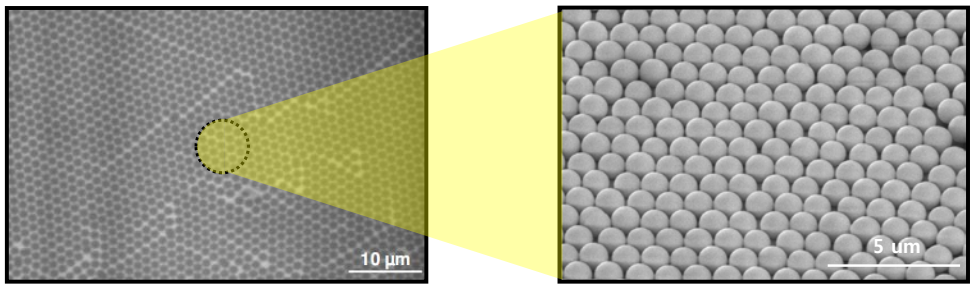

Figure 5. SEM images of the silica array template showing the local HCP pattern with defect sites such as voids.

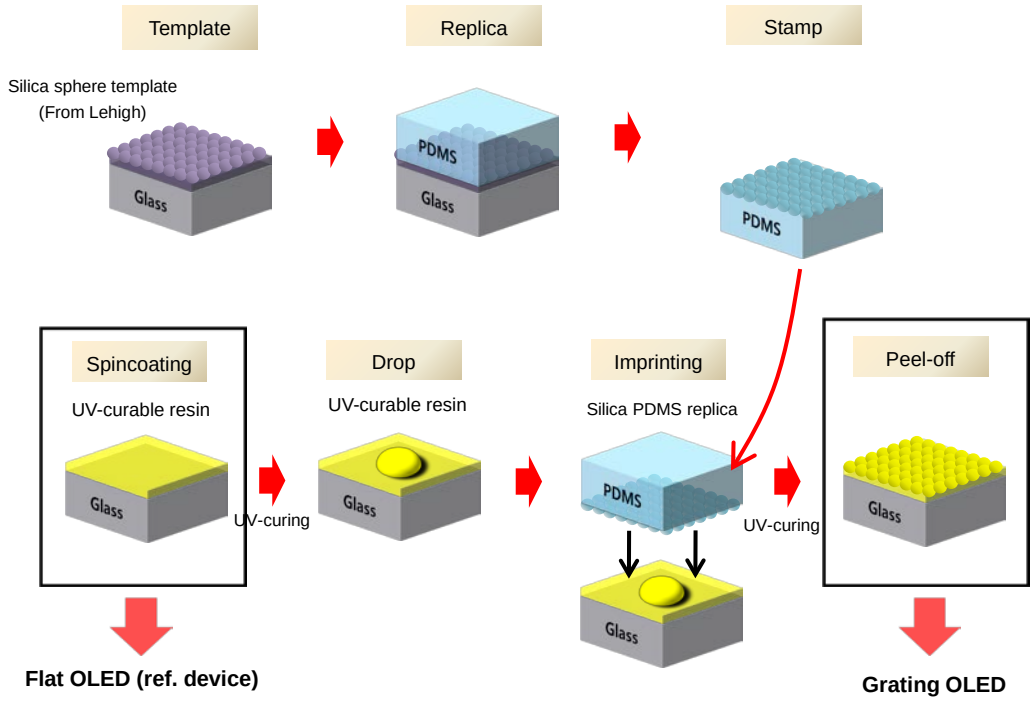

Figure 6. Illustration of imprinting process for the corrugated substrate from the silica sphere template of the Lehigh team.

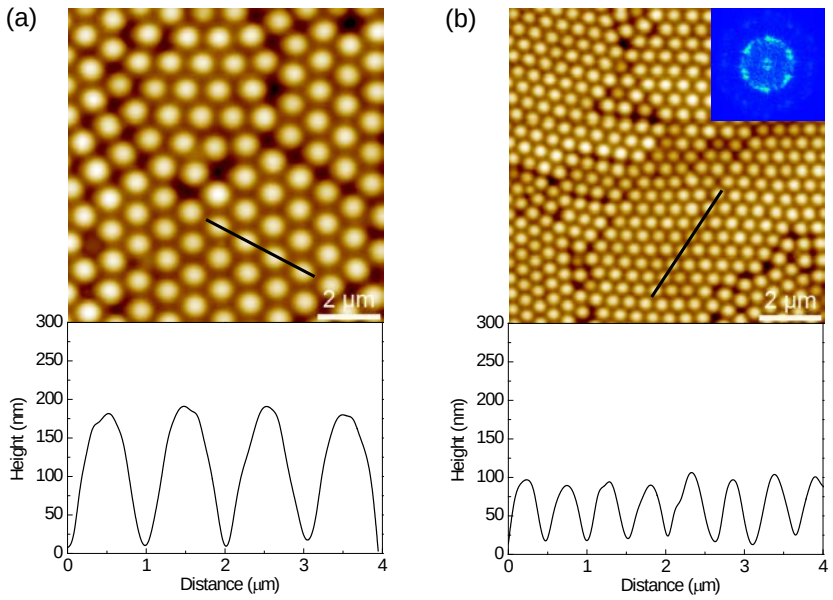

Figure 7. AFM images and line profiles on the (a) 1.0- and (b) 0.5-μm-diameter silica sphere arrays template (Dimensions, 10 × 10 μm). Inset: The FFT pattern of each image.

Figures 7(a) and (b) show the atomic force microscopy (AFM) images of the 1.0- and 0.5-μm-diameter silica sphere array templates respectively along with the fast Fourier transform (FFT) patterns as inserts. Although the local HCP areas retain the hexagonal FFT patterns, defects in the array break the long range hexagonal symmetry and generate

a ring pattern over the entire area. The FFT pattern indicates that the defective HCP array pattern forms the grating vectors in all azimuthal angles, allowing diffractions of waveguided light in all azimuthal angles. The line profiles in the AFM images show that the local HCP areas in the corrugated templates have the periodicities of 1.0 and 0.5 μm corresponding to the diameters of the silica spheres.

To fabricate the OLEDs, the following layers were deposited on the corrugated and flat resin layers coated glass substrates as shown in Fig. 6: a 120-nm-thick ITO, a 50-nm-thick NPB (N,N'-bis(naphthalene-1-yl)-N,N'-bis-(phenyl)benzidine)), a 60-nm-thick Alq_3 (tris-(8-hydroxyquinoline)-aluminum), a 1.0-nm-thick lithium fluoride (LiF), and a 100-nm-thick aluminum (Al).

III.4 Light extraction of 1.0-um-diameter silica sphere array

The typical current densities (mA/cm^2) and luminances (cd/m^2) for the devices with and without 1.0 μm grating are plotted as a function of applied voltage in Fig. 8(a). The 1.0 μm grating device shows a higher current density and a higher luminance at a constant voltage compared with the reference device. The increased current density is characteristic of a corrugated OLED because of the enhanced electric field due to non-uniformity of the organic layer thicknesses in a corrugated structure. The current (cd/A) and power efficiencies (lm/W) at a luminance of 1000 cd/m^2 are 2.6 cd/A and 1.64 lm/W for the reference device and 3.5 cd/A and 2.63 lm/W for the grating device (Fig. 4(b)). The grating device shows 35% and 60% enhancements in the current and power efficiencies compared to the reference devices.

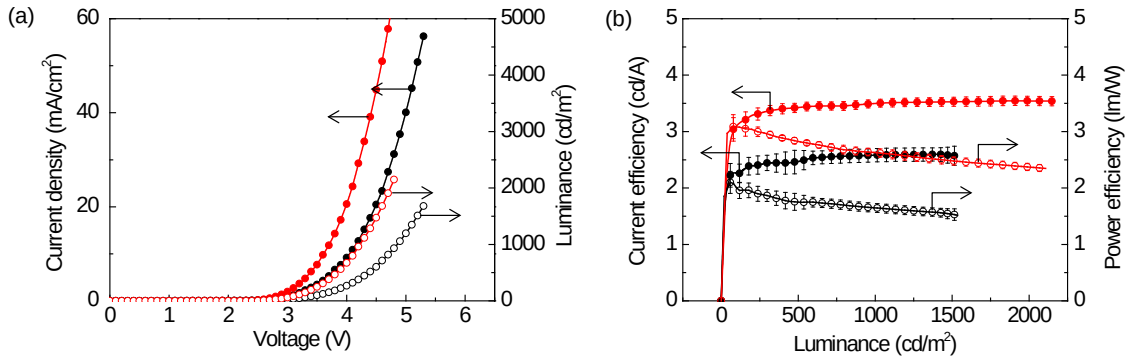

Figure 8. (a) Current density (mA/cm2) and luminance (cd/m2) and (b) Current efficiency (cd/A) and power efficiency (lm/W) for the 1.0 μm grating (red) and reference (black) devices.

III.5 Light extraction of 0.5-um-diameter silica sphere array

Figure 5(a) shows the current densities and luminances for the 0.5 μm grating device and the reference device. Similar to the 1.0 μm grating device, the 0.5 μm grating device exhibits a higher current density and higher luminance than those of the reference device. The current and power efficiencies at 1000 cd/m^2 in Figure 5(b) are 2.53 cd/A and 1.57 lm/W for the reference devices, and 4.35 cd/A and 3.2 lm/W for the grating devices, respectively. Enhancements of ~70% and 100% were achieved for the current and power efficiencies due to the 0.5 μm grating. The larger enhancement of the 0.5 μm grating

device, compared to the 1.0 μm grating device, is associated with the larger grating vector of the 0.5 μm grating.

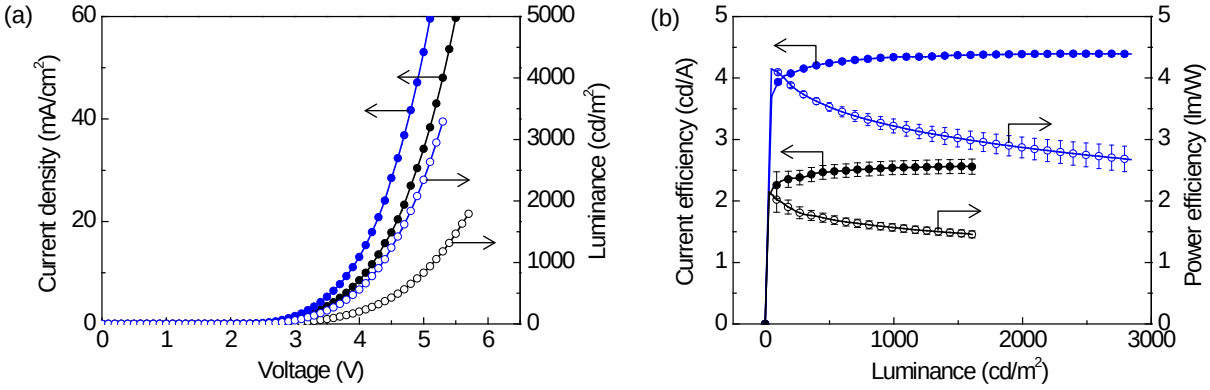

Figure 9. (a) Current density (mA/cm2) and luminance (cd/m2) and (b) Current efficiency (cd/A) and power efficiency (lm/W) for the 0.5 μm grating (blue) and reference (black) devices.

The EL spectra of the grating and reference devices at normal direction again show a broad enhancement over all emission wavelengths (Figure 6(a)). The emitting light intensities of each device for all emission angles were normalized by the intensity of each device at normal direction and displayed in Figure 6(b). The reference (black open circle) device exhibits nearly Lambertian emission pattern (black dashed line), but the 0.5 μm grating device (red open circle) shows the broader distribution, compared with the Lambertian emission pattern, particularly at around 40° which is the first-order diffraction angle of the waveguide modes (TE0 and TM0 modes) around the main emission peak of 530 nm by the grating periodicity of ~0.5 μm. It should be noted that while OLEDs fabricated on a conventional grating or photonic crystal structure with a short and long range order hexagonal symmetry give distinct butterfly wing emission patterns, the emission profile of our OLEDs fabricated on defective HCP array patterns does not show any polar- and azimuthal angle dependence because of the broadening of the periodicity and the random orientation from the defective array pattern.

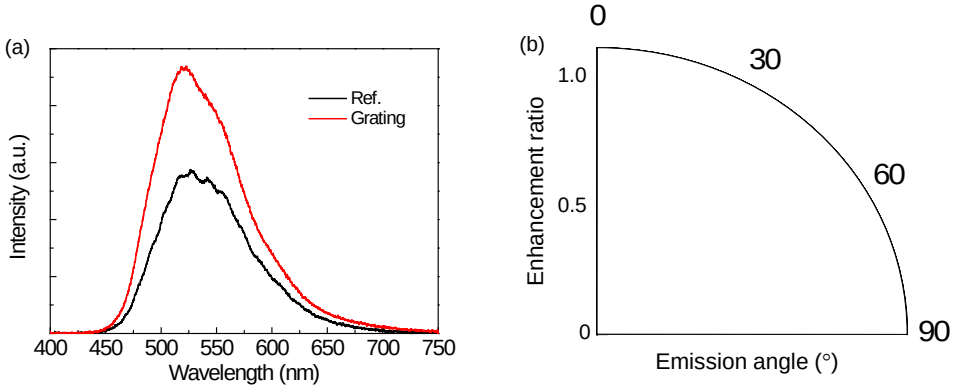

Figure 10. (a) EL spectrum of the devices with (red) and without (black) grating at normal direction (b)Angular dependence of emitting light for the 0.5 μm (red) grating and reference (black) devices. The black dashed line represents a Lambertian emission pattern.

III.6. Green phosphorescent OLEDs with 0.5-um-diameter silica sphere array

For high efficiency OLEDs, green emitting phosphorescent devices was fabricated using the following structure, as shown in Figure 11(a); a 90-nm-thick ITO as the anode layer, a 60-nm-thick 1,1-bis[(di-4-tolylamino)phenyl]cyclohexane (TAPC) as the hole transport layer, a 30-nm-thick 4,4 -N,N -dicarbazole-biphenyl (CBP) doped with 13 wt% Ir(ppy)3 as the green emitter, a 35-nm-thick 4,7-diphenyl-1,10-phenanthrolinea (Bphen) as the electron transport layer, a 1-nm-thick lithium fluoride as the electron injection layer, and a 100-nm-thick Al as the cathode layer.

Figure 11(b) shows the current density of the devices with the 500 nm grating (red) and reference (black). The grating device shows the higher current density than the reference device because of the stronger electric field in the grating device due to the partially reduced organic layer thickness. Figure 11(c) shows the current (left axis) and power efficiencies (right axis) of those devices. The current and power efficiencies at 1000 cd/m^2 are 49 cd/A and 33 lm/W for the reference devices and 78 cd/A and 72 lm/W for the grating device respectively, giving rise to 60% and 120% enhancements in the current and power efficiencies by the 500 nm grating. The greater enhancement in the power efficiency than the current efficiency is due to the lower operating voltage of the grating device at the same current density, as shown in Figure 11(b).

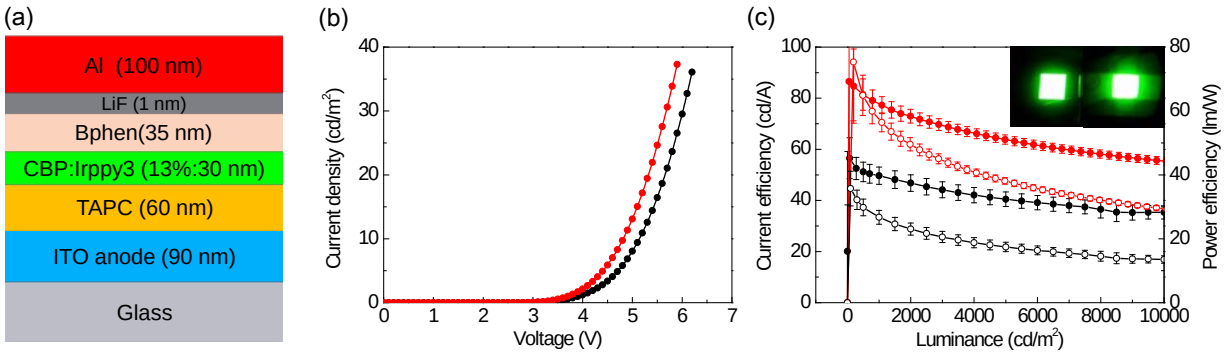

Figure 11. (a) Ir(ppy)$_3$ device structure. (b) Current density and (c) current and power efficiencies of the devices with and without 0.5 μm grating.

Figure 12(a) shows the EL spectra of the devices with the 500 nm grating (red) and reference (black) at normal direction. The intensity was enhanced over all emission wavelengths. The substrate mode can be extracted simply by attaching a hemisphere lens on back of the glass substrate. Figures 12(b) and (c) show the angular dependence of emitting light for the reference and grating devices with and without hemisphere lens. The integrated intensity over the entire angles was improved additionally by 56% and 74% for the reference and grating devices, respectively, due to extraction of the glass mode by the hemisphere lens. Finally, the power efficiencies of the 0.5 μm grating devices with lens were enhanced by a factor of ~3.7 (=$1_{\text{reference}}$×$2.2_{\text{power efficiency}}$×$1.7_{\text{lens}}$), compared with the reference device without the hemisphere lens.

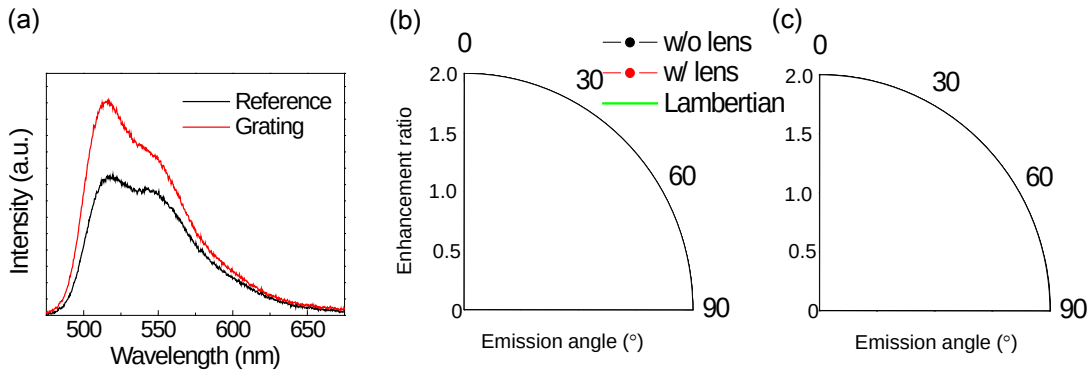

Figure 12. (a) EL spectra of the devices with (red) and without grating. Angular dependence of emitting light for (b) the reference device and (c) the grating device with and without hemisphere lens.

III.7 Green phosphorescent OLEDs with 0.4-um-diameter silica sphere array

The 400 nm grating was designed to give a higher outcoupling efficiency at normal direction than the 500 nm grating, because of its larger grating vector. However, the lower depth of the 400 nm grating than the 500 nm grating inevitably decreases the diffraction efficiency of the waveguiding light. In order to increase the depth of 400 nm grating, we make a PDMS replica from the original template by pouring PDMS material on the template and curing at 40^{o}C for 4 hours, instead of 70^{o}C for 2 hours which is a normal curing condition. Because the curing process induces the shrinkage of the PDMS materials, the lower curing temperature is preferred for maintain the same depth of the PDMS replica as that of the template. The replicated PDMS replica is used for making the device substrate with grating by imprinting process with an UV-curable resin. The depth of the corrugated resin layer was increased from 46 nm by 70^{o}C-cured replica to 58 nm by 40^{o}C-cured replica.

Figure 13(a) shows the current density (left axis) and the luminance (right axis) of the devices with 70^{o}C-cured (red) and 40^{o}C-cured (blue) 400 nm grating and reference (black). Both grating devices show the higher current density and luminance than the reference. Figure 13(b) shows the current efficiency of those devices. While the 70^{o}C-cured grating device shows ~31% enhancement in the current efficiency at the luminance of 100 cd/A, the 40^{o}C-cured grating device shows the higher enhancement of ~46%. Figure 14 (a)~(c) shows the emitting images of the reference, 70^{o}C-cured, and 40^{o}C-cured grating devices, respectively, driven at the same current density. The 40^{o}C-cured grating device having the deeper depth than the 70^{o}C-cured grating device shows the strong light scattering around the pixel, indicating the stronger outcoupling of the waveguide modes. However, the lower enhancement of the current efficiency in the 40^{o}C-cured 400 nm grating device than the 500 nm grating device is caused by the lower depth of 400 nm grating than 500 nm grating.

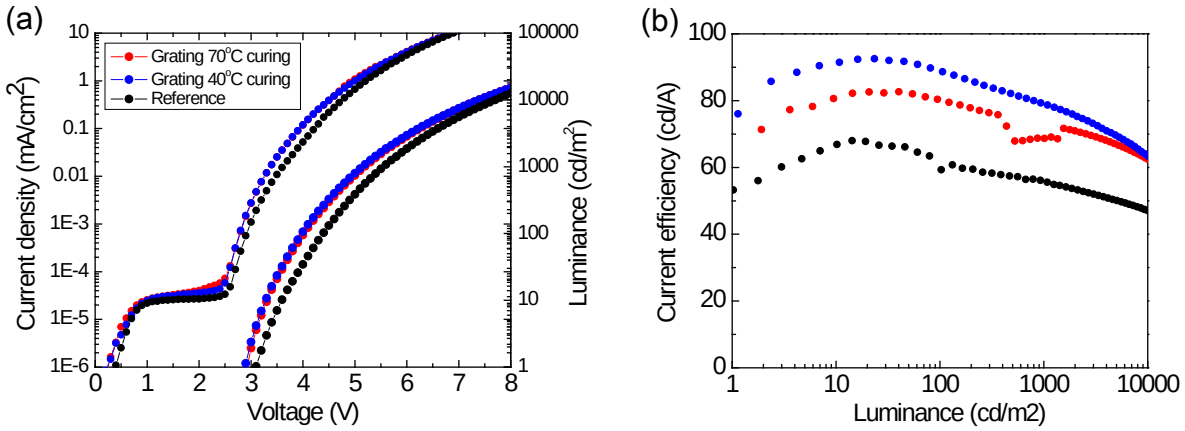

Figure 13. (a) Current density (left axis) and the luminance (right axis) and (b) current efficiency of the devices with 70°C-cured (red) and 40°C-cured (blue) 400 nm grating and reference (black).

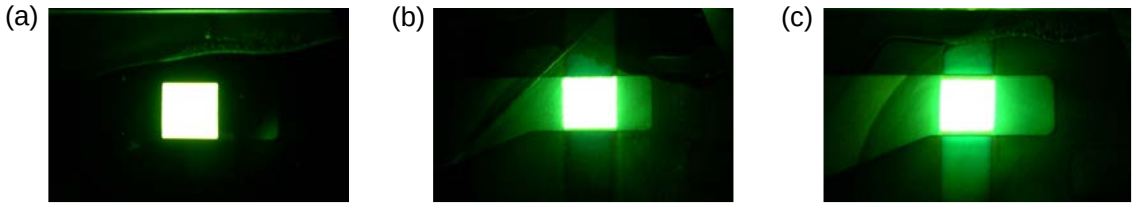

Figure 14. Emitting images of (a) the reference, (b) 70oC-cured, and (c) 40oC-cured grating devices, respectively, driven at the same current density.

C. 8 Summary of techniques to fabricate corrugated structure

Light extraction is a key for OLED to be strong candidate for lighting to replace. Among the different candidates, the corrugated grating is promising. Since 50~60% of light generated is trapped and guided by OLED stacks due to difference in refractive indices between substrate and OLED stacks. This technique can allow light to be extracted by Bragg diffraction from such periodic structure. Additionally, broad distribution of the periodicity can extract all wavelengths, which is considered another advantage compared to strong selectivity on wavelengths using photonic crystal structure. With microlens application on back side of the substrate, the outcoupling efficiency with corrugated grating structure can be very close to unity. Here, three methods to generate such structures are summarized below:

A. Rapid convective deposition of SiO_2 / PS microlens arrays

Advantages

1. Can control the aspect ratio by different size of SiO2 (100 nm, 500nm, and 1 um) and heat treatment time on PS layer, as shown in Figure 4.
2. Can extract surface plasmon and thin-flim guide mode trapped in organic/ITO layer.

3. Can extract all wavelengths in generated light by the nature of semi-randomness of the periodic structure, as called ‘defective grating’

Disadvantage

1. Still need transfer step in order to reduce its roughness
2. During the transfer step, the aspect ratio is reduced
3. Poor extraction efficiency on thin-film waveguide mode
4. Lack of large scalability; flexible PDMS stamp for transfer step is not suitable for large scale**.**

B. Spontaneously formed buckling structure

Advantage

1. Can easily generate the corrugated buckling structure by Al deposition on glass substrate
2. Can generate very broad distribution of periodicity, as shown in Figure 15.
3. Can extract surface plasmon and thin-film guide mode trapped in organic/ITO layer in all wavelengths and all azimuthal angles

Disadvantage

1. Cannot control periodicity and depth independently
2. Still need extra transferring PDMS stamp
3. Limited scalability due to PDMS stamp process

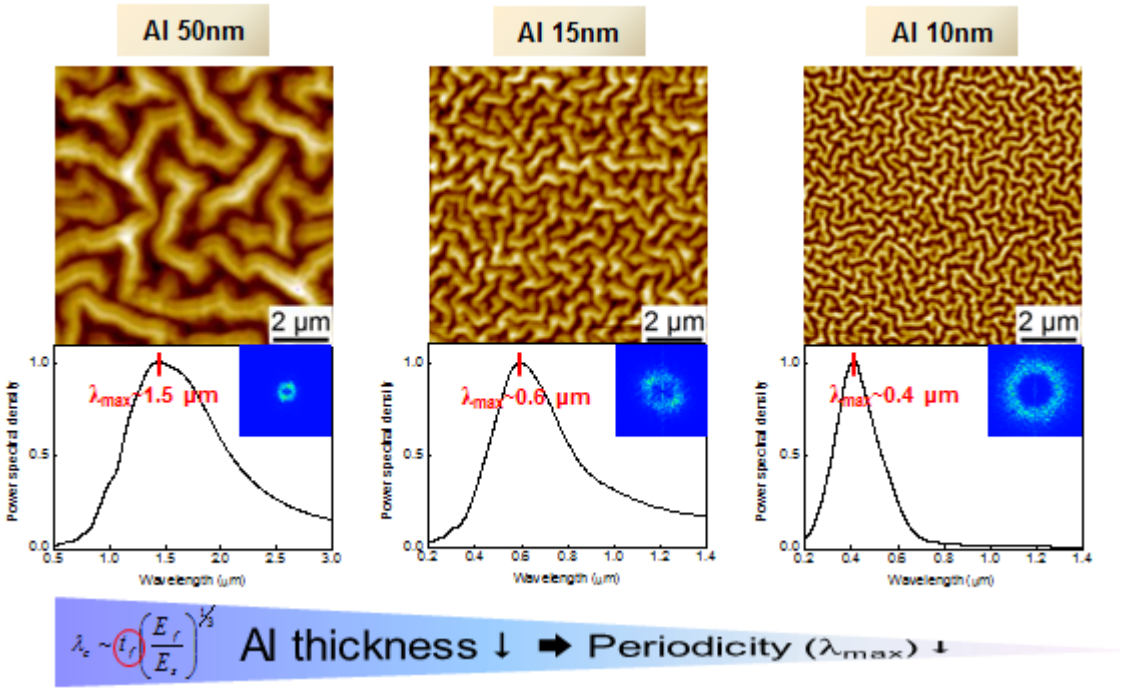

Figure 15. Corrugated buckling structure based on thickness of deposited Al layer. The higher the Al thickness, the longer the periodicity

C. Corrugated structure on high index substrate of sapphire

Advantages

1. Can control the aspect ratio by different size of SiO_2 (100 nm, 500nm, and 1 um) spheres and different etching times
2. Can generate the grating periodic structure with broad distribution of periodicity, extracting all wavelengths and all azimuthal angles, as shown in Figure 16.
3. Due to poor outcoupling of waveguide mode by corrugated structure, high index substrate is favorable for extracting only existing surface plasmon using corrugated structure
4. No extra transferring PDMS stamp is required.
5. Show more than 3 times higher in hardness than glass (2000 kg/mm^2 vs. 580 kg/mm^2)

Disadvantages

1. The sapphire substrate is more expensive than glass (5~7 times more expensive than glass).

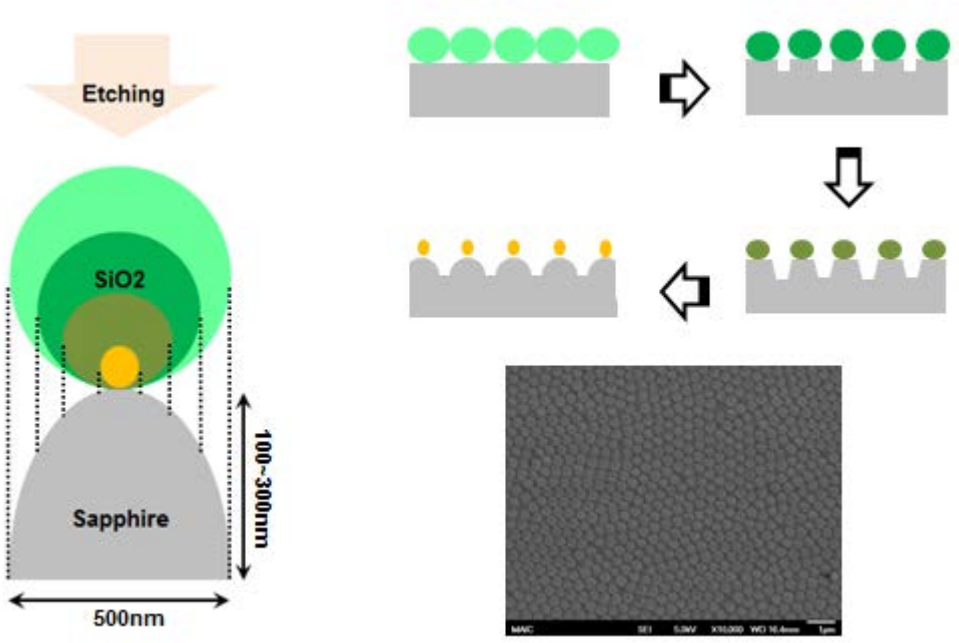

Figure 16. SEM image of top view of corrugated sapphire structure. Corrugated structure is fabricated by dry etching on SiO_2 deposited on sapphire substrate with increase in etching time. The shrunk SiO_2 is washed away by HF solution